Supplemental Information for

Two-step target recognition for the competitive inhibition activity of an anti-VEGF aptamer.

Authors

*Koh Takeuchi[1,2], Takumi Ueda[1,3], Misaki Imai[1,4], Miwa Fujisaki[1,4], Masanari Tsujimura[1,4], Yuji Tokunaga[1,2], Yutaka Kofuku[1], and *Ichio Shimada[1,5,6]

Affiliations

1. Graduate School of Pharmaceutical Sciences, The University of Tokyo, Hongo, Bunkyo, Tokyo 113-0033, Japan

2. Molecular Profiling Research Center for Drug Discovery and Cellular Molecular Biotechnology Research Institute, National Institute of Advanced Science and Technology, Aomi, Koto, Tokyo 135-0063, Japan

3. Graduate School of Pharmaceutical Sciences, Osaka University, 1-6, Yamadaoka, Suita-shi, Osaka, Japan

4. Research and Development Department, Japan Biological Informatics Consortium, Aomi 2-3-26, Koto-ku, Tokyo 135-0064, Japan.

5. Center for Biosystems Dynamics Research, RIKEN, Tsurumi, Yokohama, Kanagawa 230-0045, Japan.

6. Graduate School of Integrated Sciences for Life, Hiroshima University, 1-4-4 Kagamiyama, Higashi-Hiroshima City, Hiroshima, 739-8528, Japan

*Corresponding authors

Ichio Shimada: ichio.shimada@riken.jp

Koh Takeuchi: koh-takeuchi@mol.f.u-tokyo.ac.jp

Extended discussions for spectral simulation of t44.27 interaction with the VEGF HBD

We explored the equilibrium models and parameters that reproduce the complex behavior of the chemical shifts and signal intensities of Leu153 and Asn154 by using two-dimensional NMR spectral simulation with an exchange Monte Carlo algorithm, which reportedly allows us to consider the entire parameter space for arbitrarily complicated models. While the simulated spectra assuming only one bound state (Fig. S5A and C; left) did reproduce the characteristics of the observed CSPs (see Figure 4), those assuming two distinct bound states successfully reproduce the characteristics in the NMR titration experiment with both fast and slow exchange modes (Figs. S5B and D; right). The reproducibility was quantitatively judged from the δ values, the root-mean-square differences of the normalized chemical shifts for the calculated vs. experimental peaks. The δ value for the two-bound state model, 0.062 ppm, was significantly reduced as compared to that of the one-bound state model, 0.12 ppm (Fig. S5E). In the two-step binding mode, VEGF first binds to t44.27 with the association rate, k_{on01}, of 3.5×10^9 $M^{-1}s^{-1}$ and the dissociation constant, K_{dn01}, of 3.9 μM to form a transient complex (Table S1; left column). Subsequently, the tight complex is formed with the kinetic rate, k_{12}, of 180 s^{-1} and the equilibrium constant, K_{12}, of 6.6 (Table S1; middle column). Direct formation of the tight complex from the unbound state is much slower (k_{on02}: 7.1×10^3 $M^{-1}s^{-1}$) than the transient complex formation of two-step binding (k_{on01}: 3.5×10^9 $M^{-1}s^{-1}$) (Table S1; right column).

Supplemental Figures

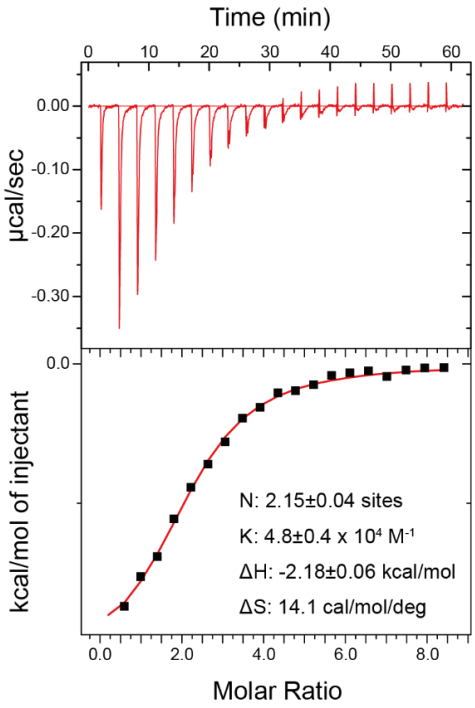

Figure S1. The ITC experiment for analyzing Ca^{2+} binding to t44.27. 2 mM $CaCl_2$ was titrated to 50 µM t44.27 to determine the thermodynamic parameter associated with the Ca^{2+} binding to t44.27.

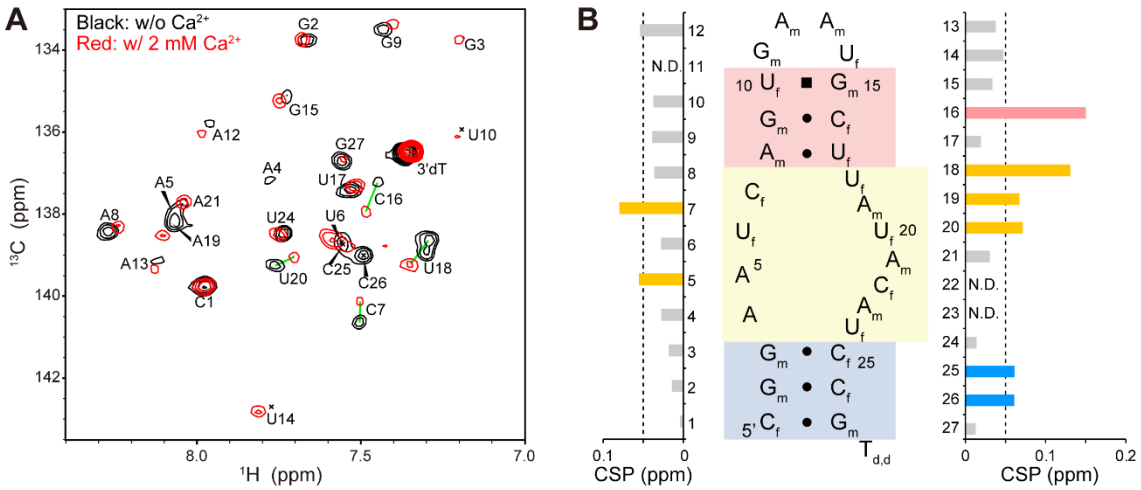

Figure S2. Ca^{2+} titration to t44.27. (A) Natural-abundance aromatic $^{1}H^{13}C$ HSQC spectrum of t44.27 in the absence (black) and presence (red) of 2 mM Ca^{2+}. Ade/Gua H8-C8, Cyt/Uri H6-C6 resonances are shown. (B) Mapping of the normalized CSPs induced by the Ca^{2+} binding to the schematic diagram of t44.27. Normalized CSP was calculated as follows: $((\Delta\delta_H)^2+(\Delta\delta_C)^2/25)^{1/2}$.

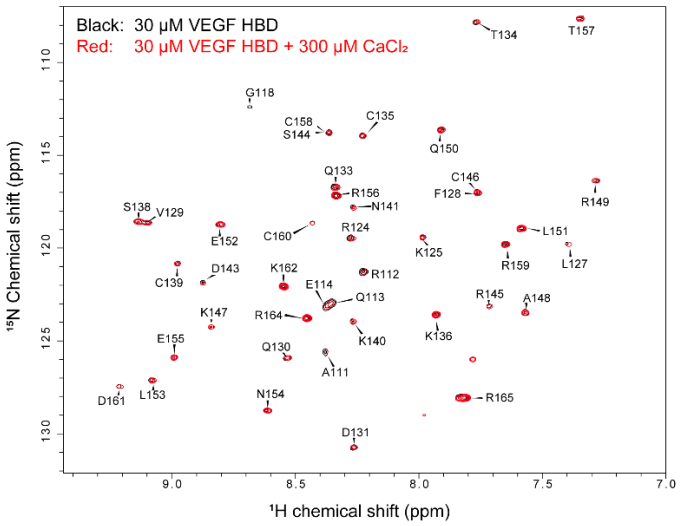

Figure S3. Ca^{2+} titration to VEGF HBD. $^{1}H^{15}N$ TROSY HSQC spectra of VEGF HBD without (black) and with (red) 300 μM Ca^{2+} are shown with the resonance assignments. Only minimal chemical shift changes were observed for the VEGF HBD resonances upon Ca^{2+} titration.

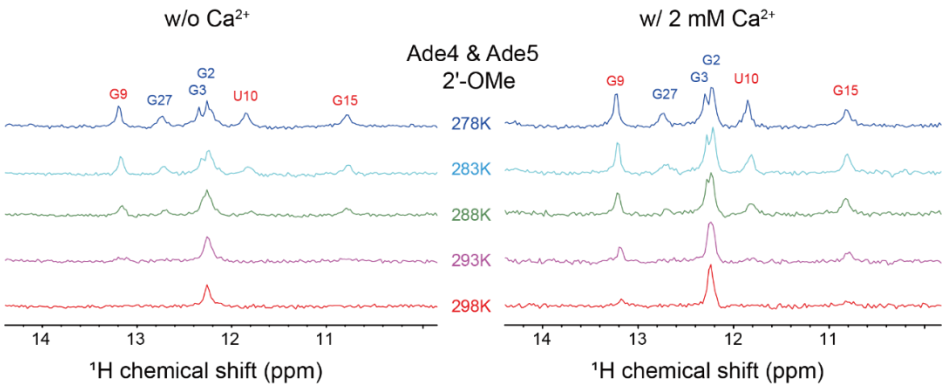

Figure S4. Temperature dependence of the imino-proton resonances of 4,5-2'-OMe. The left and right spectra show the imino-proton resonances of 4,5-2'-OMe without and with 2 mM $CaCl_2$, respectively.

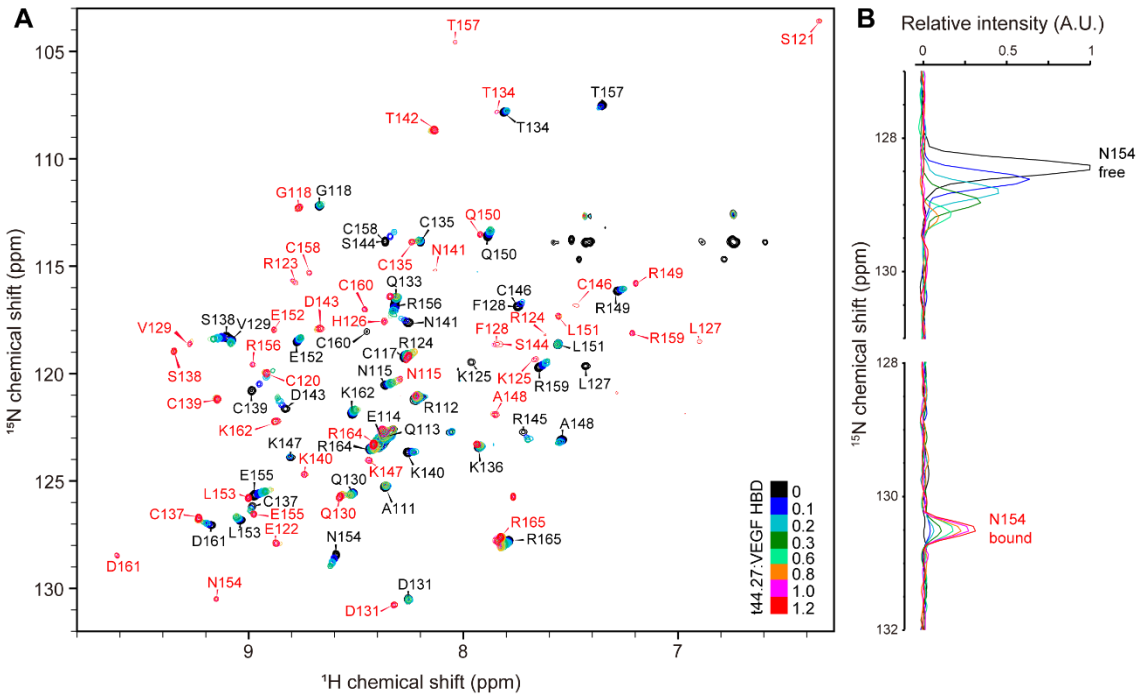

Figure S5. The $^{1}H^{15}N$ TROSY HSQC spectrum of 90 μM [*U*-$^{2}H^{15}N$] VEGF HBD upon the titration of t44.27. (A) The spectra with the indicated stoichiometry of t44.27 are shown. The assignments for the free and bound states are shown in black and red, respectively. (B) The ^{15}N slices of Asn154 resonance with the stoichiometry of t44.27 indicated in panel (A).

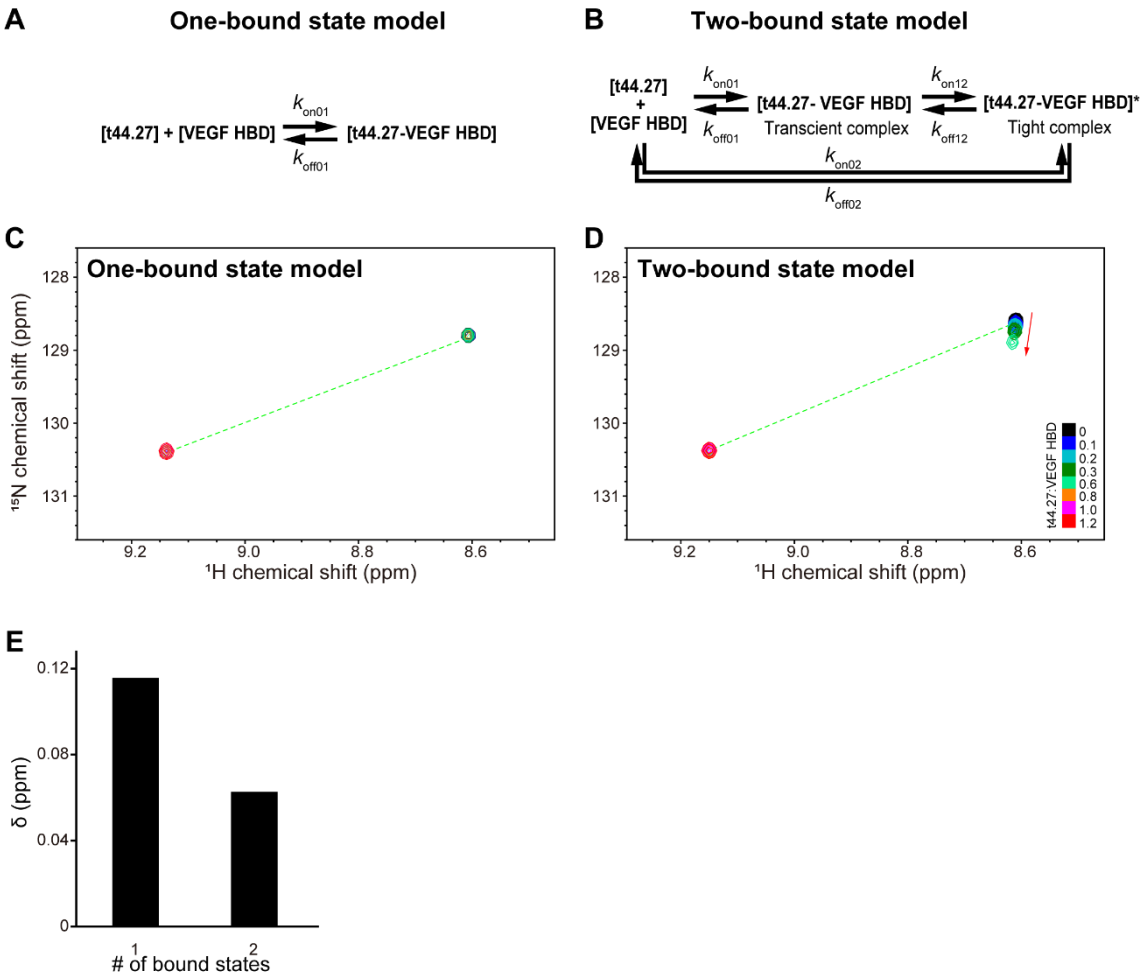

Figure S6. The spectral simulation of the VEGF HBD-t44.27 NMR titration experiment. (A and B) The (A) one- and (B) two-bound state models and the parameters assumed in the spectral simulations. (C and D) The reproduced spectra from the two-dimensional NMR line shape analyses with an exchange Monte Carlo algorithm assuming the (C) one- and (D) two-bound state models (See details in the extended discussion of t44.27 interaction with the VEGF HBD. The spectra were colored in the same way as in Figure 4. (E) The agreements of the calculated and experimental spectra evaluated by the δ values. The details of the spectral simulation are described in the extended discussions for spectral simulation of t44.27 interaction with the VEGF HBD. The kinetic and equilibrium parameters are shown in Table S1.

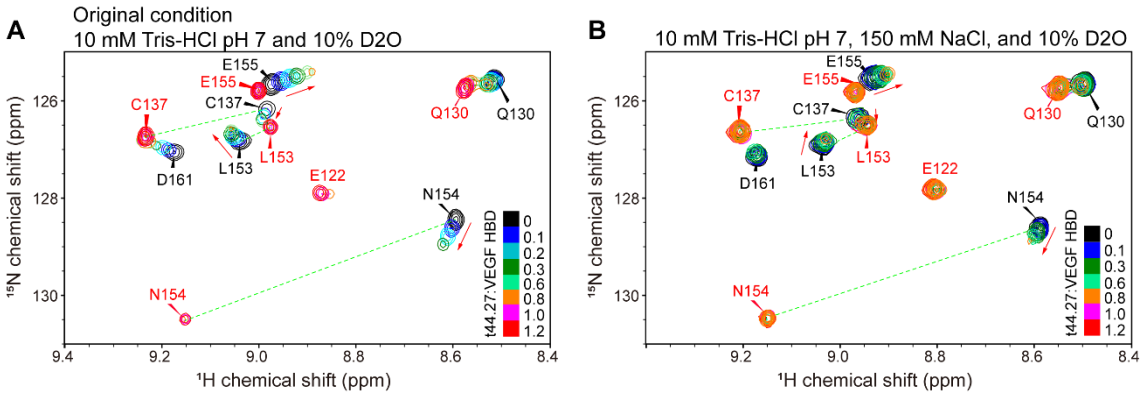

Figure S7. Two-step interaction between VEGF HBD and t44.27 in the presence of physiological salt. Expanded region of the TROSY spectrum of 90 μM [U-^{2}H,^{15}N] VEGF HBD upon titration with t44.27 at the indicated stoichiometric ratios. (A) in the absence of NaCl and (B) in the presence of 150 mM NaCl.

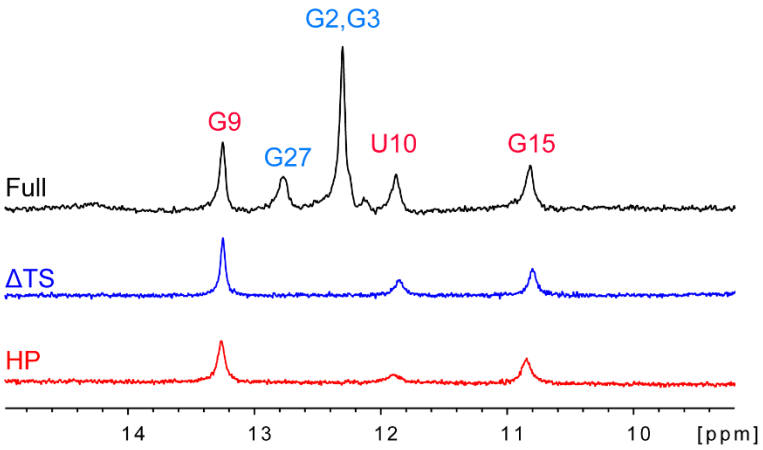

Figure S8. Imino proton resonances of the deletion constructs of t44.27. The imino proton resonances of the deletion constructs of t44.27 were recorded at 283K.

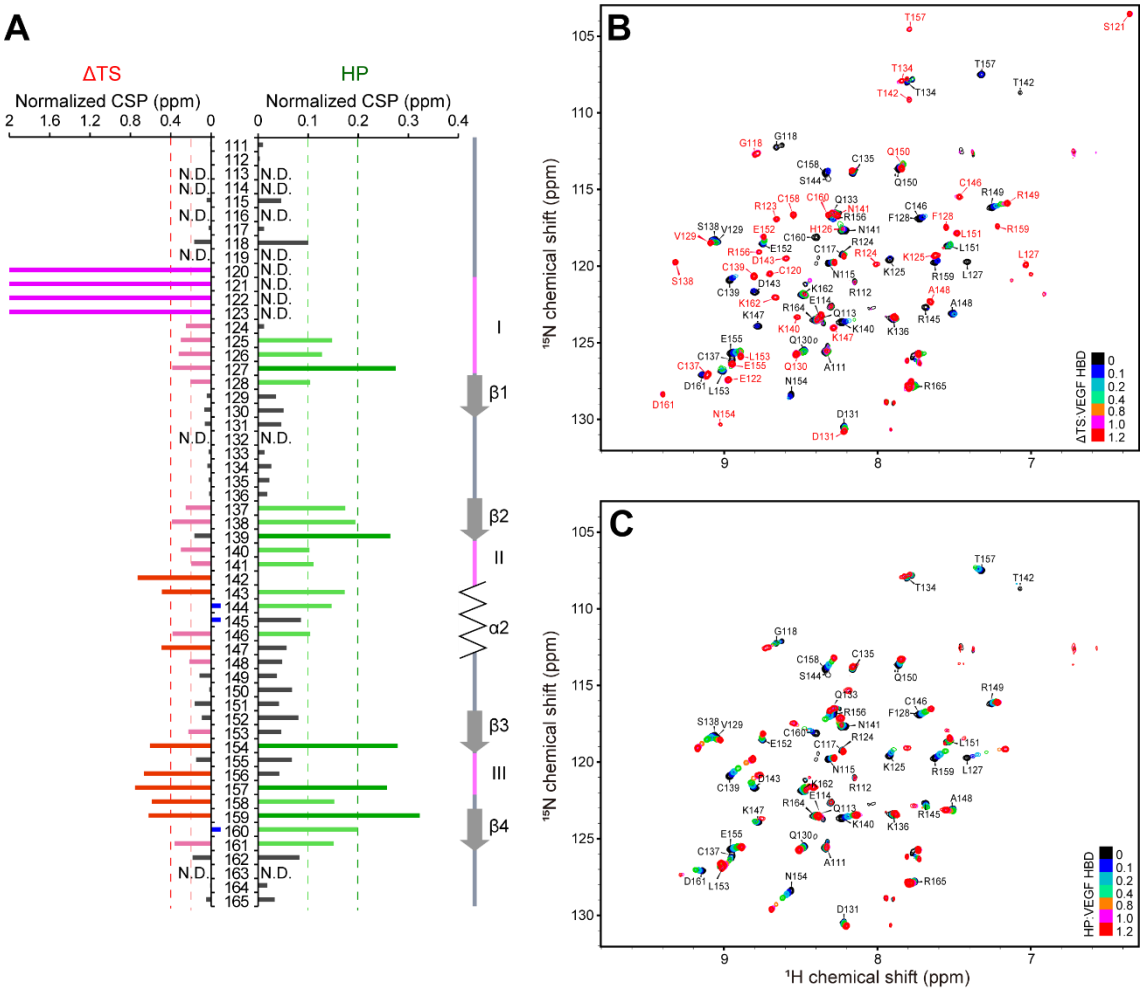

Figure S9. Titration of ΔTS and HP to [*U*-^{2}H^{15}N] VEGF HBD. (A) The normalized CSPs induced by a 1:1.2 stoichiometric amount of ΔTS and HP. The bars are colored as in Fig. 5D and E, respectively. (B and C) The ^{1}H^{15}N TROSY HSQC spectrum of 70 μM [*U*-^{2}H^{15}N] VEGF HBD upon titration of (B) ΔTS and (C) HP. The spectra with the indicated stoichiometry of the deletion construct are shown. In (B), the assignments for the free and bound states are shown in black and red, respectively. In (C), only the assignments for the free state are shown.

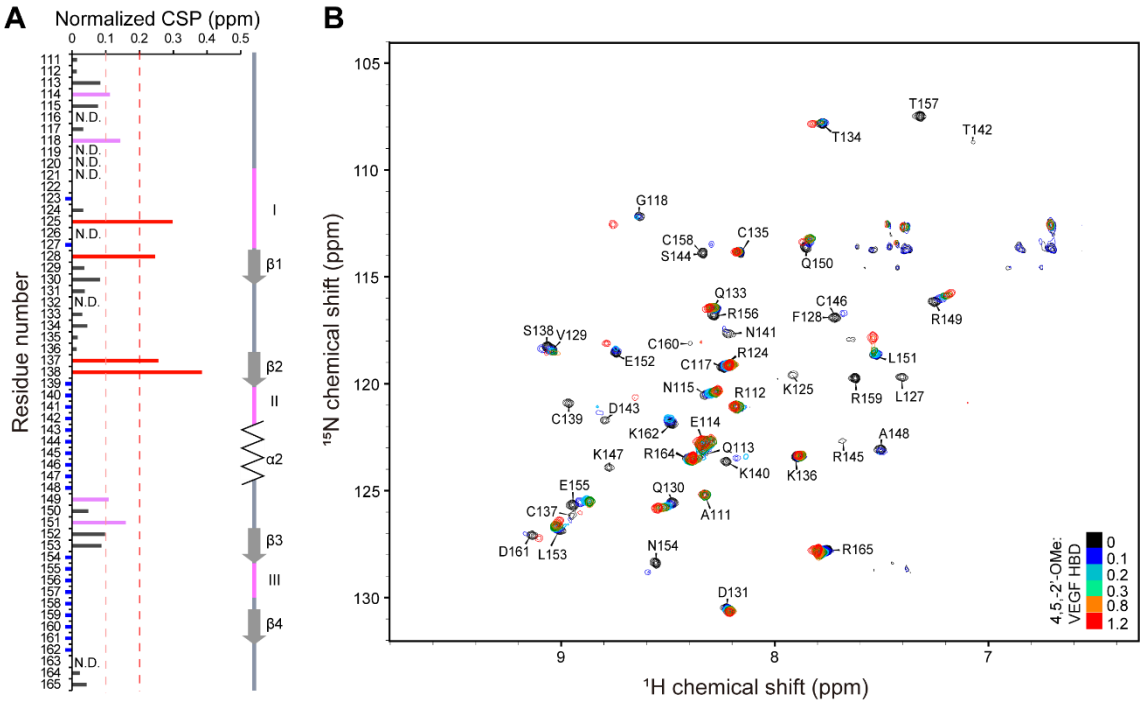

Figure S10. Titration of 4,5-2′-OMe to [*U*-^{2}H^{15}N] VEGF HBD. (A) The normalized CSPs caused by 4,5-2′-OMe titration. CSPs larger than 0.1 ppm are colored red. The residues that disappeared upon the binding to 4,5-2′-OMe are shown in blue. (B) The ^{1}H^{15}N TROSY HSQC spectra of 55 μM [*U*-^{2}H^{15}N] VEGF HBD with the indicated stoichiometry of 4,5-2′-OMe. The assignments for the free state are shown.

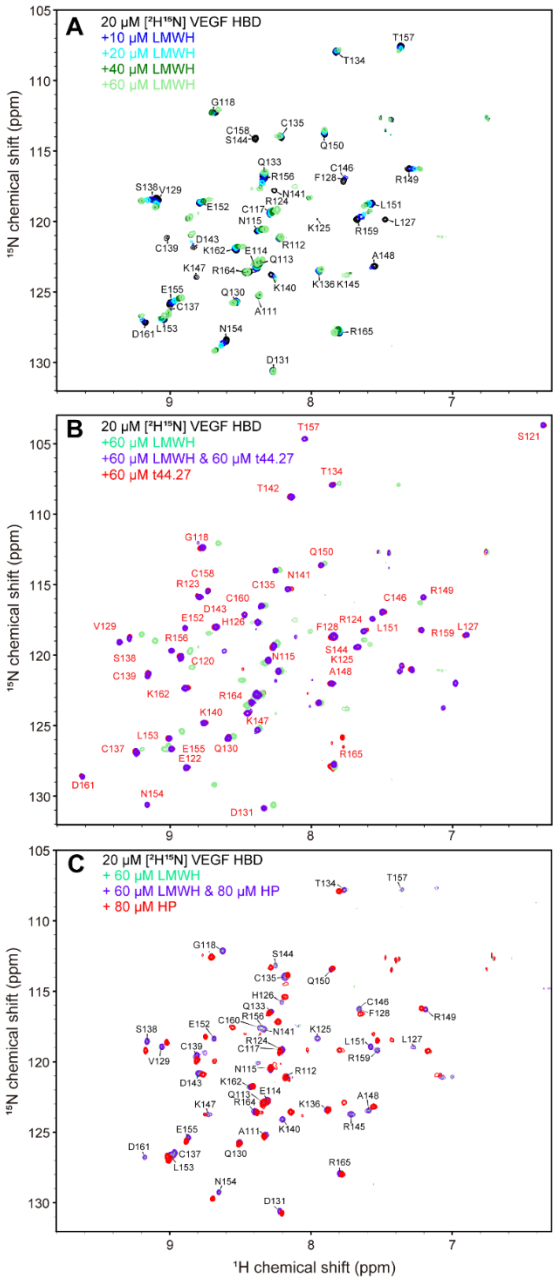

Figure S11. Heparin titration and the competition of heparin-binding by t44.27 and HP. (A) The $^{1}H^{15}N$ TROSY HSQC spectra of 20 μM [*U*-$^{2}H^{15}N$] VEGF HBD upon the titration of the indicated amount of heparin. (B and C) Addition of (B) t44.27 and (C) HP to the preformed heparin-VEGF HBD complex. The $^{1}H^{15}N$ TROSY HSQC spectra of 20 μM [*U*-$^{2}H^{15}N$] VEGF HBD with the indicated amount of heparin and RNA are shown. For comparison, the VEGF HBD spectra upon the binding to heparin and those with (B) t44.27 or (C) HP are also shown. The assignment for the free, t44.27 bound, and heparin bound states are shown in panels A, B, and C, respectively.

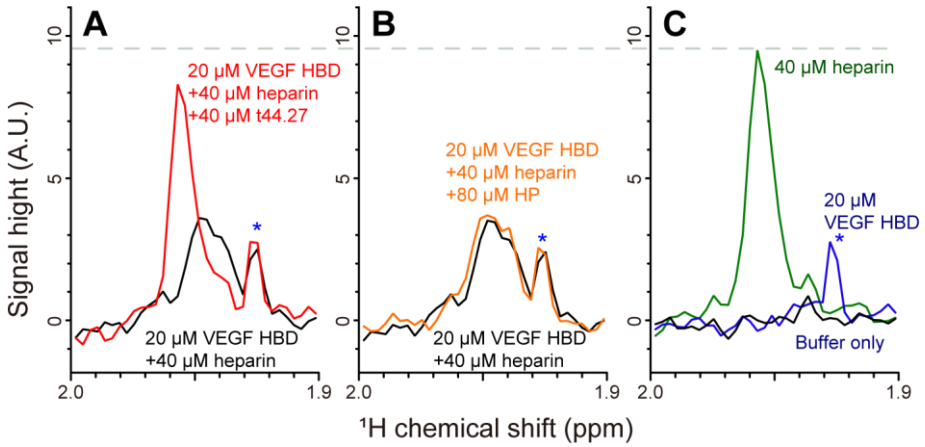

Figure S12. The recovery of heparin signal by competitive inhibition of binding. (A) ^{1}H 1D spectrum of 40 μM haparin in the presence of 20 μM [*U*-^{2}H] VEGF HBD (black) and in the presence of both 20 μM [*U*-^{2}H] VEGF HBD and 40 μM t44.27 (red). (B) ^{1}H 1D spectrum of 40 μM haparin in the presence of 20 μM [*U*-^{2}H] VEGF HBD (black) and in the presence of both 20 μM [*U*-^{2}H] VEGF HBD and 80 μM HP (orange). (C) Reference ^{1}H 1D spectra of 40 μM heparin (green), 20 μM [*U*-^{2}H] VEGF HBD (blue), and NMR buffer (black).

Table S1. The dissociation constants and exchange rates obtained from the spectral simulation assuming the two-bound states model.

The deviations of estimated values are shown in parentheses. Definitions of kinetic parameters are shown in Figure S5. Definitions of equilibrium parameters are as follows; $K_{d01} = k_{off01}/k_{on01}$, $K_{12} = k_{11}/k_{21}$, and $K_{d02} = k_{off02}/k_{on02}$

k_{on01}	3.5 (0.96-13) $\times 10^9$ $M^{-1}s^{-1}$	k_{12}	180 (40-800) s^{-1}	k_{on02}	0.71 $\times 10^3$ (< 5.3 $\times 10^6$) $M^{-1}s^{-1}$
k_{off01}	1.3 (0.17-11) $\times 10^4$ s^{-1}	k_{21}	28 (5-150) s^{-1}	k_{off02}	0.0041 (<3.3) s^{-1}
K_{d01}	3.9 (1.0-15) $\times 10^{-6}$ M	K_{12}	6.6 (3.1-14)	K_{d02}	5.8 (2.1-16) $\times 10^{-7}$ M